REPORT

SUPERCONDUCTIVITY

# Electric field control of superconductivity at the $LaAlO_3/KTaO_3(111)$ interface

Zheng Chen[1]†, Yuan Liu[1]†, Hui Zhang[2]†, Zhongran Liu[3], He Tian[3], Yanqiu Sun[1], Meng Zhang[1], Yi Zhou[4,5,6]*, Jirong Sun[4,5,7]*, Yanwu Xie[1,8]*

The oxide interface between $LaAlO_3$ and $KTaO_3(111)$ can harbor a superconducting state. We report that by applying a gate voltage ($V_G$) across $KTaO_3$, the interface can be continuously tuned from superconducting into insulating states, yielding a dome-shaped $T_c$-$V_G$ dependence, where $T_c$ is the transition temperature. The electric gating has only a minor effect on carrier density but a strong one on mobility. We interpret the tuning of mobility in terms of change in the spatial profile of the carriers in the interface and hence, effective disorder. As the temperature is decreased, the resistance saturates at the lowest temperature on both superconducting and insulating sides, suggesting the emergence of a quantum metallic state associated with a failed superconductor and/or fragile insulator.

Controlling superconductivity with an electric field is intriguing for both fundamental research and potential applications (*1*–*11*). Analogous to the case of semiconducting field-effect transistors (*9*), the two-dimensional (2D) carrier density $n_{2D}$ of a superconductor can be tuned by applying an external gating voltage $V_G$. The attainable tuning ability can be estimated as $\delta n_{2D} = \varepsilon_0\varepsilon_r V_G/et$, where $\varepsilon_0$ is the vacuum permittivity, $e$ is the elementary charge, and $\varepsilon_r$ and $t$ are the dielectric constant and the thickness of the dielectric material, respectively. To achieve prominent tuning of the superconductivity, particularly a transition from superconducting to insulating states, a $\delta n_{2D}$ value that is comparable with $n_{2D}$ is generally needed. However, the $n_{2D}$ value of most superconductors is very high and far beyond the capability of typical electric gating (~$10^{14}$ $cm^{-2}$ or lower) (*9*). Therefore, it has been a long-standing challenge to control superconductivity electrostatically.

With recent advances in material fabrication and tuning technology, prominent tunings of superconductivity have been experimentally realized for a few systems, including oxide interfaces (*1*, *6*, *7*), electric-double-layer interfaces (*2*–*4*, *8*, *10*, *11*), and magic-angle graphene superlattices (*5*). These tunings were achieved by pushing the superconducting layer to an ultrathin limit to reduce $n_{2D}$, by developing technologies such as electric-double-layer gating to improve tuning ability (*3*, *11*), or— most often—by both (*2*, *12*). The tuning parameter in all these systems is $n_{2D}$.

$KTaO_3$(KTO) shares many common properties with $SrTiO_3$(STO) (*13*). In comparison with the well-known $LaAlO_3$(LAO)/STO interface (*14*), a 2D electron gas was observed at the LAO/KTO(001) (*15*) and $LaTiO_3$/KTO(001) (*16*) interfaces, but no superconductivity was reported. Superconductivity was observed at the electric-double-layer-gated KTO(001) surface; however, the transition temperature $T_c$ was low (~0.05 K) (*4*). Very recently, it was found that the EuO/KTO(111) and LAO/KTO(111) interfaces can be superconducting with a $T_c$ of up to ~2 K (*17*).

Here we demonstrate that the superconductivity at the LAO/KTO(111) interface can be tuned by applying $V_G$, and that, rather than $n_{2D}$, the key tuning parameter appears to be mobility, which can be associated with an "effective disorder."

We grew LAO films by pulsed laser deposition on 0.5-mm-thick single-crystalline KTO(111) substrates (*18*). The surfaces of these films were atomically flat (fig. S1). The microstructure of the interface was assessed by scanning transmission electron microscopy (STEM), which shows that LAO is homogeneous and amorphous (Figs. 1, A and B). The lack of epitaxial growth can be ascribed to the large lattice mismatch (*15*): The cubic lattice constants are 0.379 and 0.399 nm for LAO and KTO, respectively. The LAO films themselves are highly insulating; the conductance is in the KTO layer near the interface. A sketch of the field-effect device is shown in Fig. 1C. The gating voltage $V_G$ is applied between the conducting LAO/KTO layer and a silver paste electrode at the back of the KTO. The active area of the device was patterned into a Hall bar configuration (Fig. 1D). All transport measurements in this study were performed on the same device.

The occurrence of superconductivity with a midpoint $T_c$ ~2 K can be clearly seen in the temperature-dependent sheet resistance $R_{sheet}(T)$ (Fig. 1E). The thickness of the superconducting layer is estimated to be ~4 nm, and the estimated coherence length is ~18.8 nm (fig. S3). The comparison of these two length scales suggests a 2D superconductor. The 2D nature of the superconductivity can be further justified by the nonlinear current-voltage response [$V \sim I^3$ dependence indicates a typical Berezinskii-Kosterlitz-Thouless (BKT) transition as shown in fig. S4], the large anisotropy of the upper critical field $H_{c2}$ (fig. S3), and the magnetic-field–angle dependence of $R_{sheet}(T)$ (fig. S5).

The normal-state Hall resistance measured at 8.6 K (Fig. 1F) demonstrates that the charge carriers are electrons rather than holes, and the carrier density $n_{2D}$ is ~$8.5 \times 10^{13}$ $cm^{-2}$. This value is much higher than that of a typical LAO/STO interface (*1*, *19*–*22*) and is not expected to be appreciably tuned by applying $V_G$. As an estimation, adopting a low-temperature $\varepsilon_r$ of 5000 for KTO (*23*), a 300-V variation in $V_G$ can induce a $\delta n_{2D}$ value of only ~$1.7 \times 10^{13}$ $cm^{-2}$ (~20% of the total $n_{2D}$). Given that $\varepsilon_r$ in the interface region can be severely degraded by growth-induced defects and $V_G$-caused electric fields, the real attainable density $\delta n_{2D}$ is expected to be even smaller, and thus insufficient to produce any prominent tuning. However, contrary to this expectation, the transport properties of the device were strongly tuned. When sweeping $V_G$ from 150 V to −200 V, the device transits continuously from a superconductor to an insulator, and the normal-state resistance varies by more than two orders of magnitude (Fig. 2A). The $V_G$-tuned superconductor-insulator transition can also be convincingly seen in the evolution of the current-voltage behavior (Fig. 3). The midpoint $T_c$ derived from the $R_{sheet}(T)$ values (Fig. 2A and figs. S6 and S7) exhibits an interesting dome-shaped dependence on $V_G$ (Fig. 2B). This dependence resembles the dome-shaped superconducting phase diagram observed in many other systems (*1*, *4*, *11*), but the underlying mechanism is different because $n_{2D}$ in the present device is not changed much by $V_G$, as



[1]Interdisciplinary Center for Quantum Information, State Key Laboratory of Modern Optical Instrumentation, and Zhejiang Province Key Laboratory of Quantum Technology and Device, Department of Physics, Zhejiang University, Hangzhou 310027, China. [2]School of Integrated Circuit Science and Engineering, Beihang University, Beijing, 100191, China. [3]Center of Electron Microscope, State Key Laboratory of Silicon Materials, School of Materials Science and Engineering, Zhejiang University, Hangzhou, 310027, China. [4]Beijing National Laboratory for Condensed Matter Physics and Institute of Physics, Chinese Academy of Sciences, Beijing 100190, China. [5]Songshan Lake Materials Laboratory, Dongguan, Guangdong 523808, China. [6]Kavli Institute for Theoretical Sciences and CAS Center for Excellence in Topological Quantum Computation, University of Chinese Academy of Sciences, Beijing 100190, China. [7]School of Physical Sciences, University of Chinese Academy of Sciences, Beijing 100049, China [8]Collaborative Innovation Center of Advanced Microstructures, Nanjing University, Nanjing 210093, China.
†These authors contributed equally to this work.
*Corresponding author. Email: yizhou@iphy.ac.cn (Y. Z.); jrsun@iphy.ac.cn (J. S.); ywxie@zju.edu.cn (Y. X.)

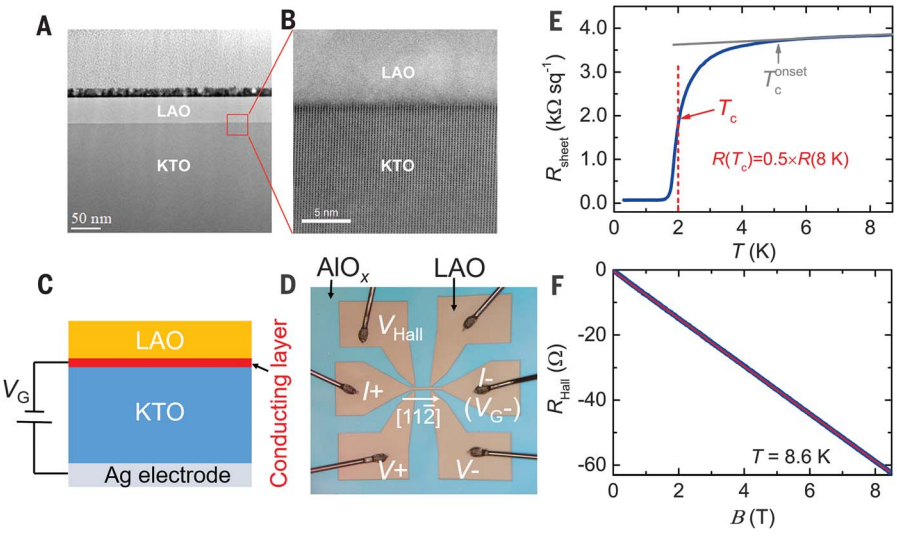


**Fig. 1. Characterization of the LAO/KTO(111) device.** (**A** and **B**) STEM images of a 40-nm LAO/KTO sample show that the LAO film is homogeneous and amorphous. (**C**) Cross-sectional view of the device structure. (**D**) Photograph of a typical device with bonded Al contacting wires. The device was fabricated in a six-probe Hall bar configuration. The conducting region is limited to the LAO/KTO interface (Hall bar area). The outside insulating region was obtained by coating amorphous $AlO_x$ as a hard mask. The central Hall bar bridge is 20 μm in width and 100 μm in length (between $V^+$ and $V^-$). The current drain ($I$-) and the gating contact to the interface ($V_G$-) share the same probe. The electrical current flows along the [11$\bar{2}$] crystal axis. (**E**) Dependence of $R_{sheet}$ on temperature and (**F**) dependence of $R_{Hall}$ on the magnetic field for the 20-nm LAO/KTO device at $V_G$ = 0.

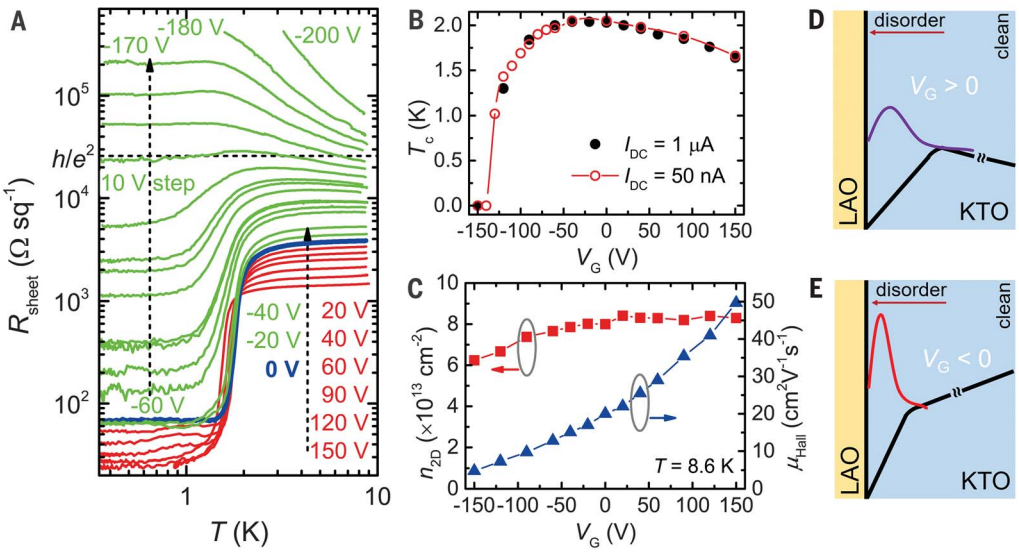


**Fig. 2. Electric field control of transport properties.** (**A**) Temperature-dependent $R_{sheet}(T)$, (**B**) midpoint $T_c$, and (**C**) carrier density $n_{2D}$ and mobility $\mu_{Hall}$ at different $V_G$ values. The dashed line in (A) indicates the position of the quantum resistance $h/e^2$. Two sets of data measured using different DC currents are shown in (B). The black filled circles represent the data measured in the same run as the Hall-effect measurements. (**D** and **E**) Schematic diagrams of the operations for $V_G$ > 0 and $V_G$ < 0, respectively. The purple and red lines represent the electron envelope wave function perpendicular to the interface, matching the potential well (thick solid lines) at the corresponding $V_G$. A higher degree of disorder is expected in the region closer to the interface.

shown below. It is worth mentioning that the present gate-tuned $T_c$ does not obey the scaling relation $T_c \propto (V_G\text{-}V_c)^{2/3}$ that was observed in LAO/STO and attributed to $V_G$-induced carrier density changes (*1*) (fig. S8).

To characterize these tunable effects, we carried out normal-state Hall-effect measurements for different $V_G$ values. To avoid any hysteresis effect, these measurements were made just before the $R_{sheet}(T)$ measurement for each $V_G$. The derived $n_{2D}$ and Hall mobility $\mu_{Hall}$ are summarized in Fig. 2C. The data in the $V_G$ range between 150 and −40 V are informative. In this range, $n_{2D}$ changes only slightly, whereas $\mu_{Hall}$ decreases from ~50 to ~15 cm$^2$ V$^{-1}$ s$^{-1}$. This strongly suggests that $V_G$ mainly modulates the carrier mobility; we interpret this finding in terms of $V_G$ tuning the effective disorder in the conducting layer, which in turn modulates the electron scattering rate and thereby the charge carrier mobility. The relatively fast decrease in $n_{2D}$ for $V_G$ < −40 V is an indication of disorder-induced localization and cannot be attributed to $\delta n_{2D}$ produced by the capacitance effect (note that varying $V_G$ between −40 and −150 V can induce a $\delta n_{2D}$ ~0.6 × 10$^{13}$ cm$^{-2}$ at best, which is only 37% of the experimentally observed value). It is convenient to characterize the effective disorder by the value of $k_Fl$, where $k_F$ is the Fermi wave vector and $l$ is the electron mean-free path. By applying the data for $R_{sheet}$ (8 K) and $n_{2D}$ (8.6 K), we found that $k_Fl$ was tuned from 17.5 ($k_Fl \gg 1$, clean) to 0.4 ($k_Fl \lesssim 1$, strongly disordered) by varying $V_G$ (from 150 to −200 V, fig. S10). The corresponding value of the Drude conductivity is $\sigma_D^{(2D)} \sim (5-18) \times e^2/h$ at $k_Fl > 5$.

As $V_G$ varies from 150 to −80 V, the superconducting layer thickness decreases gradually from above 6 nm to below 2 nm (fig. S11). Supported by this observation, the $V_G$-induced modulation of effective disorder can be understood as sketched in Fig. 2, D and E: The electron envelope wave function is pushed away or compressed toward the interface by $V_G$ > 0 or < 0. Because the disorder strength usually has a gradient from the disordered interface to the ordered interior, a variation in the spatial distribution of electrons equivalently causes a change in the average effective disorder. A similar modulation of the effective disorder by applying $V_G$ was observed previously in the LAO/STO interface (*19*, *20*, *22*). Whereas the disorder effect generally plays a secondary role in LAO/STO, it dominates in our LAO/KTO device. This difference can be attributed to the following three factors: First, the dielectric constant of KTO (*23*) is smaller than that of STO (*1*); second, the $n_{2D}$ of LAO/KTO is larger than that of LAO/STO (*1*, *19*–*22*);

third, compared with LAO/STO (*19*–*22*), LAO/KTO has a much higher effective disorder, as indicated by the low-mobility $\mu_{Hall}$, probably owing to the more disordered interface and the thinner electron gas.

Considering the framework above, the tuning achieved by $V_G$ is concluded to be a natural disorder-driven effect. Disorder-driven superconductor-to-insulator quantum phase transitions (QPTs) have been intensely studied in disordered films (*24*–*27*). Compared with that configuration, the present device is distinctive because its effective disorder can be continuously tuned by $V_G$. Notably, although we observed an apparent superconductor-insulator transition and a large variation in $R_{sheet}$, a true superconducting ground state ($R_{sheet} = 0$) is absent. As shown in Fig. 2A [see also the Arrhenius plot of $R_{sheet}(T)$, fig. S12], on the superconducting side, the resistance $R_{sheet}(T)$ does not reach zero even at the lowest temperatures and saturates below ~1 K. Measured with or without filters, the residual resistance is unchanged, which excludes the possibility of radiation thermalization (fig. S13). This intrinsic residual resistance, whose value spans a wide range from ~20 to above $10^3$ ohms/square, can be tuned continuously with $V_G$.

The superconductivity in our system is verified not only by the large drop of the resistance at $T_c$, but also by the existence of a critical current. As illustrated in Fig. 3, at $T = 0.35$ K, the critical current is ~8.3 μA at $V_G = 100$ V and decreases as $V_G$ decreases and eventually vanishes at the superconductor-insulator transition. For gating voltage $V_G$ from 150 to −130 V, the resistance at temperatures below $T_{BKT}$ (~1.7 K at $V_G = 0$) is measured by applying a DC current smaller than the critical current, where the linear *I*-*V* dependence (inset of Fig. 3) indicates an intrinsic ohmic resistance. As the temperature is lowered, the resistance falls at first and then saturates at a value that can be orders of magnitude smaller than its normal-state value and can be continuously tuned by varying $V_G$ (Fig. 2A). The resistance saturation begins at a relatively high temperature (~1 K) (Fig. 2A), which together with the $V_G$ dependence (Fig. 2A) and the linear *I*-*V* relation (Fig. 3, inset) excludes the possibility of Joule heating. Residual resistance saturation in the superconducting state has been observed in diverse 2D superconducting systems (*8*, *19*, *24*, *28*–*30*). The associated superconductors are called "failed superconductors" in the literature (*30*). The corresponding ground state is called an anomalous or quantum metallic state, whose origin is still under vigorous debate (*24*, *27*, *29*–*31*). The saturated resistance in the insulating state can be ascribed to the applied electric field–induced electron percolation on top of the insulating state. In this sense, the insulating state is fragile and can be called a "fragile insulator."

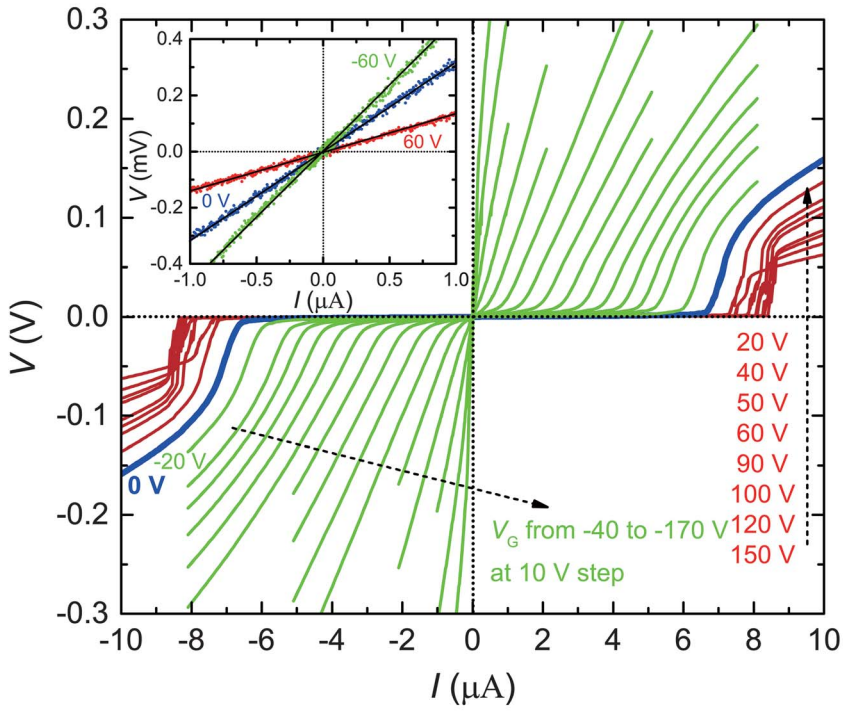


**Fig. 3. Current (*I*)-voltage (*V*) behaviors of the central 20 μm by 100 μm bridge for $V_G$ varying from 150 to −170 V.** The measurements were performed at $T = 0.35$ K. The evolution from superconducting to insulating states is indicated from the gradual variation in the superconducting critical current. Inset: Three typical linear *I*-*V* dependences in the low current range.

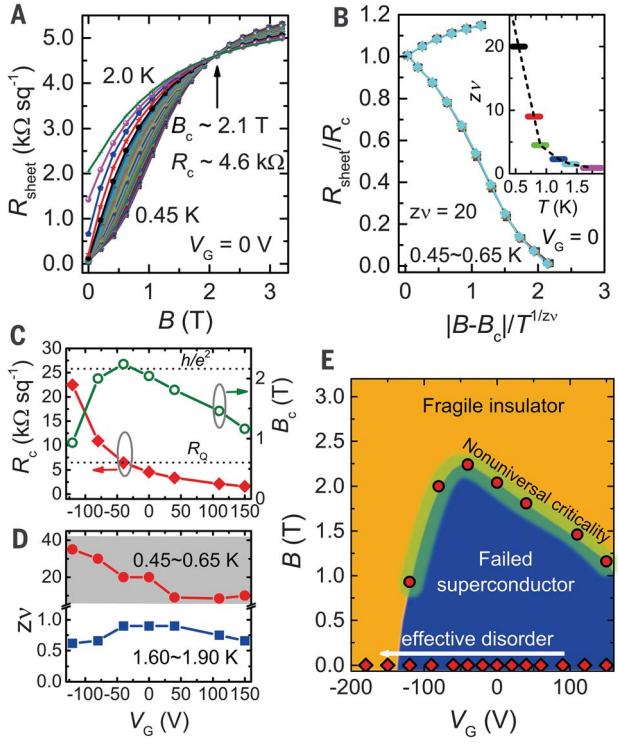


**Fig. 4. $V_G$ modulation during a QPT driven by a magnetic field perpendicular to the interface.** (**A**) Dependence of $R_{sheet}$ on the magnetic field *B* at fixed temperatures below 2 K. These curves were replotted from the temperature-dependent $R_{sheet}(T)$ data shown in fig. S5A. (**B**) Scaling of the data in 0.45 K ≤ *T* ≤ 0.65 K with respect to a single variable $|B - B_c|/T^{1/z\nu}$, with $z\nu = 20$. The inset shows the $z\nu$ values needed to scale the data in different temperature regimes (thick lines). (**C**) Dependences of $R_c$ and $B_c$ on $V_G$. The dashed lines indicate the positions of the quantum resistance $h/e^2$ and the pair quantum resistance $R_Q$. (**D**) Dependence of $z\nu$ on $V_G$ for 0.45 K ≤ *T* ≤ 0.65 K (circles) and 1.60 K ≤ *T* ≤ 1.90 K (squares). The gray shadow highlights the large uncertainty in determining the $z\nu$ values in the low-temperature regime (see fig. S15). (**E**) A schematic $V_G$-*B* phase diagram for $T = 0$. The red dots correspond to the green circles in Fig. 4C; the red diamonds correspond to the data shown in Fig. 2A ($B = 0$). For $B > B_c$, in the insulating phase, $R_{sheet}$ still saturates to a finite value (fig. S16).

Resistance saturation in the insulating state, although rare, was observed previously in disordered ultrathin Ga films (*32*), disorder-tuned LAO/STO interfaces (*19*), and graphene in a high magnetic field (*33*).

In disordered 2D superconductors, the magnetic-field–driven superconductor-to-insulator QPTs (*24*, *34*) is an interesting issue. The ability to continuously tune the effective disorder (from $k_F l \gg 1$ to $k_F l \sim 1$) in a single device enables us to monitor the disorder-dependent evolution of such QPTs. Figure 4A shows the plots of $R_{sheet}$ as a function of a perpendicular magnetic field $B$ for various temperatures below 2 K, at $V_G = 0$. These plots cross at approximately a single point, indicating a magnetic-field–driven superconductor-to-insulator QPT (*25*, *26*). The crossing point corresponds to the critical field $B_c$ and the critical resistance $R_c$. To study the criticality of such QPTs, we analyzed the data with the scaling relation $R_{sheet}(\delta, T) = R_c f(\delta T^{-1/z\nu})$, where $\delta = |B - B_c|$, $f$ is an arbitrary function with $f(0) = 1$, $z$ is the dynamical critical exponent, and $\nu$ is the correlation length exponent (*7*, *25*, *27*, *34*, *35*). A notable observation is that the exponent product $z\nu$ is not universal but diverges with decreasing temperature (Fig. 4B and its inset and figs. S14 and S15). A similar divergent $z\nu$ was observed previously in a few experimental studies (*35*, *36*) and has been discussed in recent theoretical work (*30*, *37*). One plausible explanation is that the disorder in the conducting layer gives rise to superconducting granularities, for which local quantum phase fluctuations, rather than large-scale superconducting fluctuations, are relevant (*38*).

As summarized in Fig. 4, C and D, by sweeping $V_G$ from 150 to −120 V, the critical resistance $R_c$ is tuned continuously from ~1/4 to ~4 $R_Q$ (where $R_Q = h/4e^2 \approx 6.45$ kilohm is the quantum resistance of the Cooper pairs), and the critical magnetic field $B_c$ exhibits a dome-shaped dependence on $V_G$, which evokes the dome-shaped $T_c$-$V_G$ relation in the absence of an external magnetic field (Fig. 2B). All $z\nu$ values in the high-temperature regime (1.60 to 1.90 K) are within $0.7 \pm 0.2$, which is similar to those observed in STO-based 2D superconducting interfaces (*1*, *7*). In contrast, the $z\nu$ values in the low-temperature regime (0.45 to 0.65 K) are extremely large (divergent), implying that nonuniversal criticality generally exists. Finally, on the basis of all these observations, a schematic $V_G$-$B$ phase diagram is produced in Fig. 4E.

In addition to the results presented in this report, we have fabricated and measured a total of 30 samples with different carrier densities and mobilities and found that the effective disorder-controlled tuning is quite general, although the tuning ability does depend on sample details, particularly the mobility (e.g., figs. S17 and S18). Our experiments show that a prominent low-temperature resistance saturation and a strong $V_G$-induced tuning tend to occur in low-mobility samples. Furthermore, strongly anisotropic transport behaviors have been observed in low-mobility samples (fig. S18). We emphasize that these anisotropic behaviors are different from the anisotropic superconductivity observed in EuO/KTO(111), because the latter is associated with high-mobility samples (*17*). Our work demonstrates that LAO/KTO(111) is an ideal platform to explore the rich physics of disordered 2D superconductors.

## REFERENCES AND NOTES


1. A. D. Caviglia *et al.*, *Nature* **456**, 624–627 (2008).
2. A. T. Bollinger *et al.*, *Nature* **472**, 458–460 (2011).
3. K. Ueno *et al.*, *Nat. Mater.* **7**, 855–858 (2008).
4. K. Ueno *et al.*, *Nat. Nanotechnol.* **6**, 408–412 (2011).
5. Y. Cao *et al.*, *Nature* **556**, 43–50 (2018).
6. C. Richter *et al.*, *Nature* **502**, 528–531 (2013).
7. J. Biscaras *et al.*, *Nat. Mater.* **12**, 542–548 (2013).
8. Y. Saito, Y. Kasahara, J. Ye, Y. Iwasa, T. Nojima, *Science* **350**, 409–413 (2015).
9. C. H. Ahn, J.-M. Triscone, J. Mannhart, *Nature* **424**, 1015–1018 (2003).
10. J. T. Ye *et al.*, *Nat. Mater.* **9**, 125–128 (2010).
11. J. T. Ye *et al.*, *Science* **338**, 1193–1196 (2012).
12. C. H. Ahn *et al.*, *Science* **284**, 1152–1155 (1999).
13. J. R. Thompson, L. A. Boatner, J. O. Thomson, *J. Low Temp. Phys.* **47**, 467–475 (1982).
14. A. Ohtomo, H. Y. Hwang, *Nature* **427**, 423–426 (2004).
15. H. Zhang *et al.*, *ACS Appl. Mater. Interfaces* **9**, 36456–36461 (2017).
16. K. Zou *et al.*, *APL Mater.* **3**, 036104 (2015).
17. C. Liu *et al.*, *Science* **371**, 716–721 (2021).
18. Materials and methods and figs. S1 to S18 are available as supplementary materials.
19. Z. Chen *et al.*, *Nat. Commun.* **9**, 4008 (2018).
20. Z. Chen *et al.*, *Nano Lett.* **16**, 6130–6136 (2016).
21. N. Reyren *et al.*, *Science* **317**, 1196–1199 (2007).
22. C. Bell *et al.*, *Phys. Rev. Lett.* **103**, 226802 (2009).
23. Y. Fujii, T. Sakudo, *J. Phys. Soc. Jpn.* **41**, 888–893 (1976).
24. A. M. Goldman, *Int. J. Mod. Phys. B* **24**, 4081–4101 (2010).
25. N. Marković, C. Christiansen, A. M. Mack, W. H. Huber, A. M. Goldman, *Phys. Rev. B* **60**, 4320–4328 (1999).
26. A. Yazdani, A. Kapitulnik, *Phys. Rev. Lett.* **74**, 3037–3040 (1995).
27. N. Mason, A. Kapitulnik, *Phys. Rev. Lett.* **82**, 5341–5344 (1999).
28. A. W. Tsen *et al.*, *Nat. Phys.* **12**, 208–212 (2016).
29. C. Yang *et al.*, *Science* **366**, 1505–1509 (2019).
30. A. Kapitulnik, S. A. Kivelson, B. Spivak, *Rev. Mod. Phys.* **91**, 011002 (2019).
31. I. Tamir *et al.*, *Sci. Adv.* **5**, eaau3826 (2019).
32. C. Christiansen, L. M. Hernandez, A. M. Goldman, *Phys. Rev. Lett.* **88**, 037004 (2002).
33. J. G. Checkelsky, L. Li, N. P. Ong, *Phys. Rev. Lett.* **100**, 206801 (2008).
34. M. P. A. Fisher, *Phys. Rev. Lett.* **65**, 923–926 (1990).
35. Y. Xing *et al.*, *Science* **350**, 542–545 (2015).
36. Y. Saito, T. Nojima, Y. Iwasa, *Nat. Commun.* **9**, 778 (2018).
37. B. Spivak, P. Oreto, S. A. Kivelson, *Phys. Rev. B* **77**, 214523 (2008).
38. B. Sacépé, M. Feigel'man, T. M. Klapwijk, *Nat. Phys.* **16**, 734–746 (2020).
39. Y. Xie, Data for "Electric field control of superconductivity at the $LaAlO_3/KTaO_3$(111) interface," Zenodo (2021); https://doi.org/10.5281/zenodo.4626213.


## ACKNOWLEDGMENTS


We thank S. A. Kivelson, H. Y. Hwang, H. Yao, and F. C. Zhang for fruitful discussions. Hall-bar devices were made at the Micro-Nano Fabrication Center of Zhejiang University. **Funding:** This work was supported by the National Key Research and Development Program of China (grant nos. 2017YFA0303002, 2016YFA0300202, 2016YFA0300204, 2016YFA0300701); National Natural Science Foundation of China (grant nos. 11934016, 11774306); the Strategic Priority Research Program of Chinese Academy of Sciences (grant no. XDB28000000); the Key R&D Program of Zhejiang Province, China (2021C01002, 2020C01019); and the Fundamental Research Funds for the Central Universities of China. J.S. thanks the support of the Science Center of the National Science Foundation of China (52088101) and the Project for Innovative Research Team of National Natural Science Foundation of China (11921004). **Author contributions:** Z.C., Y.L., H.Z., Y.S., and M.Z. prepared the samples; Z.C., Y.L., and Y.X. performed the transport measurements; Z.L. and H.T. performed the STEM measurements; and Y.Z., J.S., and Y.X. analyzed the data and wrote the manuscript with input from all authors. **Competing interests:** The authors declare no competing interests. **Data and materials availability:** Data for all graphs presented in this paper are available from Zenodo (*39*).


## SUPPLEMENTARY MATERIALS

science.sciencemag.org/content/372/6543/721/suppl/DC1
Materials and Methods
Figs. S1 to S18
References (*40*)


29 March 2020; accepted 2 April 2021
10.1126/science.abb3848

Science

# Electric field control of superconductivity at the LaAlO/KTaO(111) interface

Zheng ChenYuan LiuHui ZhangZhongran LiuHe TianYanqiu SunMeng ZhangYi ZhouJirong SunYanwu Xie

*Science*, 372 (6543), • DOI: 10.1126/science.abb3848

**Controlling interfacial superconductivity**

The interface between the oxides LaAlO and KTaO(111) has been shown to superconduct at temperatures up to 2 Kelvin. Chen *et al.* show that this superconductivity can be controlled with electric fields. As they tuned the gating voltage, the researchers observed a dome-shaped variation of the superconducting critical temperature. This variation could not be ascribed to the change in carrier density, but rather seemed to reflect the change in the mobility of the carriers.

*Science*, this issue p. 721







*Science* (ISSN 1095-9203) is published by the American Association for the Advancement of Science. 1200 New York Avenue NW, Washington, DC 20005. The title *Science* is a registered trademark of AAAS.